IJME

Int. J. of Applied Mechanics and Engineering, 2025, vol.30, No.4, pp.1-17
DOI: 10.59441/ijame/210536

MOGA-BASED OPTIMIZATION AND PERFORMANCE COMPARISON OF PLAIN AND MULTI-LOBE HYDRODYNAMIC JOURNAL BEARINGS

N.B. Ahire[1] and D.D. Deshmukh[2*]
Mechanical Engineering Department, MET's IOE, BKC, Nasik, SPPU, Pune, India
[1]E-mail: ahirenitin0105@gmail.com
[2]E-mail: dhirgajanan@gmail.com

Choosing the best hydrodynamic journal bearing (HJB) involves a complex multi-objective optimization challenge that requires balancing load carrying capacity (LCC), friction loss, oil film temperature increase, and dynamic stability. This research utilizes the multi objective genetic algorithm (MOGA) to optimize plain, two-lobe, three-lobe, and four-lobe journal bearings under different operating conditions. The variable parameters of HJBs, including rotational speed, clearance, L/D ratio, load were taken into account. The optimization process utilized Pareto-based selection, simulated binary crossover and Gaussian mutation techniques to determine the optimal bearing choice. The three-lobe bearing proved to be the most suitable choice based on its superior load-carrying capacity, minimal temperature rise, reduced friction loss, and overall stability performance. The findings reveal that the four-lobe bearing excels in LCC, while the plain and two-lobe bearings are advantageous for their simple design and low manufacturing costs. These results offer valuable insights for engineers and designers when choosing the most appropriate bearing type based on specific operational needs and performance trade-offs.

Key words: HJBs, multi objective optimization, load carrying capacity, friction loss, stability.

1. Introduction

The current study seeks to assess the effectiveness of different journal bearing designs, specifically plain, two-lobe, three-lobe, and four-lobe, by examining key performance indicators such as LCC, temperature increase, friction loss, and stability score. HJBs are widely used in rotating machinery because they offer low wear, excellent damping properties, and can support substantial loads under diverse operating conditions [1, 2]. These bearings function according to the principle of hydrodynamic lubrication, where a thin lubricant film separates the rotating shaft from the bearing surface, thus preventing direct metal contact and reducing friction and wear [3, 4]. This lubrication method is essential for high-speed and high-load applications, including turbines, compressors and internal combustion engines, ensuring smooth and dependable operation [5, 6]. The pressure field created by the lubricant film, which is affected by factors like lubricant viscosity, bearing geometry, and clearance, is crucial to the bearing's performance [6].

Although traditional plain bearings are straightforward in their design, they often become unstable at higher rotational speeds, resulting in issues such as significant friction losses, increased temperatures and dynamic instabilities like oil whirl [8, 9]. These drawbacks have spurred the creation of more advanced bearing designs, notably multi-lobe bearings, which provide improved LCC, stability and resistance to dynamic instabilities [8, 9]. Multi-lobe bearings, including two-lobe, three-lobe and four-lobe types, distribute the load more uniformly across several arcs or lobes, enhancing performance in high-speed and heavy-load scenarios [10]. The effectiveness of these bearings is influenced by design factors such as clearance, the length-to-diameter (L/D) ratio, and the number of lobes, which affect the pressure and thickness of the lubricant film [7, 11]. To address the multi-objective optimization challenges in journal bearing design, advanced techniques such as MOGAs have gained prominence. MOGAs enable the simultaneous optimization of bearing design variables such as eccentricity ratio, L/D ratio, speed, load, clearance, and oil viscosity, facilitating a comprehensive evaluation of performance metrics [2, 8]. Advancements in Computational Fluid Dynamics

* To whom correspondence should be addressed

(CFD) and the use of nanolubricants, such as those containing TiO_2 nanoparticles, have further enhanced tribological performance by reducing wear and improving heat dissipation [1, 11]. CFD techniques have also enabled the optimization of groove shapes and oil film thickness, leading to improved heat dissipation and more efficient lubricant flow management [12]. The optimization of surface textures on twin-grooved two-lobe hydrodynamic journal bearings using genetic algorithms, achieving significant improvements in dynamic performance parameters such as damping, stiffness, and a *195.55%* increase in threshold speed [13]. Reliability-based design optimization of rotor-bearing systems, incorporating surrogate modeling techniques, effectively optimized shaft diameter and oil temperature under uncertainty, achieving *99%* reliability in vibration amplitude and stability threshold [14]. A multi-objective optimization of camshaft bearings using NSGA-II and entropy-weighted TOPSIS reduced friction loss and wear while enhancing the average minimum oil film thickness and overall tribological performance [15].

This comprehensive analysis seeks to identify the most suitable bearing design that balances these parameters under varying operating conditions, thereby providing valuable insights for optimizing bearing performance in practical applications. The Fig.1 shows various parameters and bearing types for optimum bearing selection.

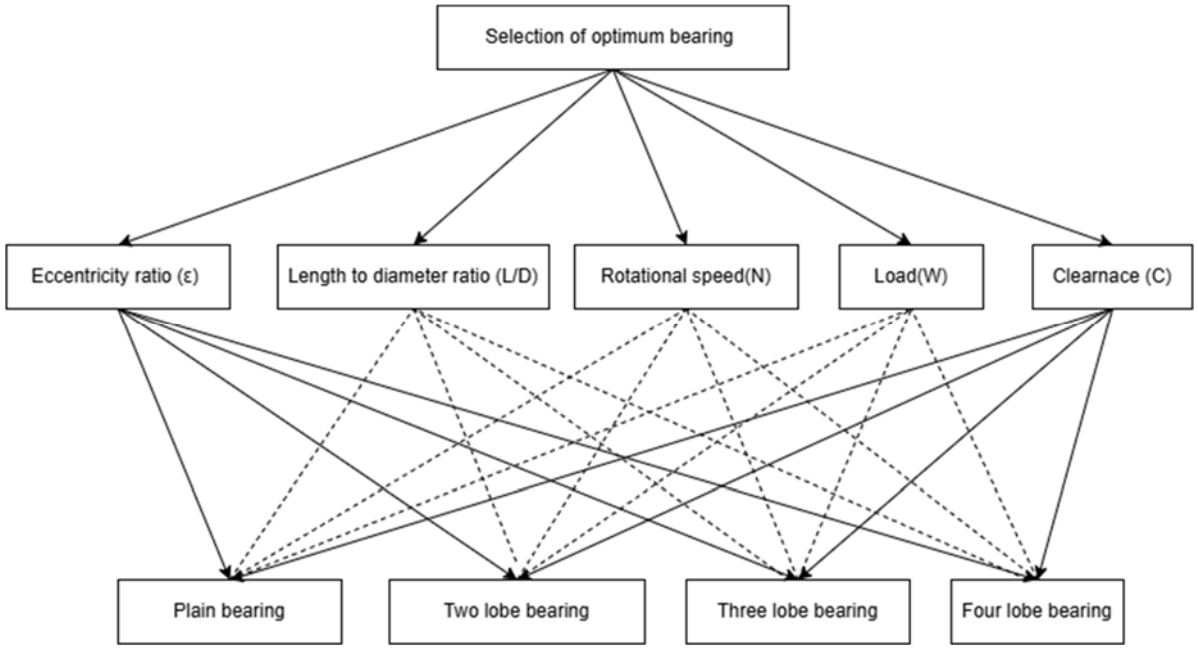

Fig.1. Parameters and types of bearings relation.

2. Mathematical model

A schematic representation of the journal bearing geometry is shown in Fig.2. It depicts a journal of radius *r* rotating inside a bearing of radius *R*, with an eccentricity *e* along the line of centres, inclined at an attitude angle ϕ. The journal rotates at an angular speed *N* and is subjected to an external load *W*. In this study, the mathematical model is adopted based on a varying eccentricity ratio ε within the range of $0.4 \le \varepsilon \le 0.8$, operating at speeds ranging from *100* to *1500 RPM*. This model is particularly effective for estimating the performance of average-speed bearings commonly used in turbines and other rotating machinery.

For a steadily loaded journal bearing, the non-dimensional form of the Reynolds equation, as presented is given [16]:

$$\frac{\partial}{\partial\theta}\left(\bar{h}_0^3\frac{\partial\bar{P}_o}{\partial\theta}\right)+\left(\frac{D}{L}\right)^2+\frac{\partial}{\partial\bar{z}}\left(\bar{h}_0^3\frac{\partial\overline{P_o}}{\partial\bar{z}}\right)=\frac{\partial\bar{h}_0}{\partial\theta}. \tag{2.1}$$

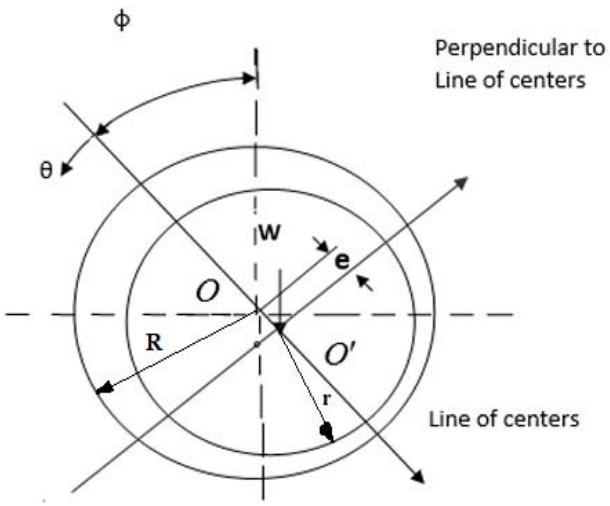

Fig.2. Journal bearing geometry.

The oil film thickness h can be expressed as:

$$h = C\left(1 + e\varepsilon\cos\theta\right) \tag{2.2}$$

where C is the radial clearance and θ is the angle measured from the line of centres. It can be noticed that the minimum film thickness occurs at $\theta = 180°$ $\left(i.e. h_{\min} = C - e\right)$ and the maximum film thickness occurs at $\theta = 0°$ $\left(i.e. h_{max} = C + e\right)$.

The modelling process involves calculating the Somerfield number *S* for given value of *N* and *W*, using initial values of *C*, oil viscosity and bearing dimensions:

$$S = \left(\frac{R}{C}\right)^2 \left(\frac{\mu DLN}{W}\right) \tag{2.3}$$

where μ is the oil viscosity, *D* is the bearing diameter and *L* is the bearing length. Then, the eccentricity ratio ε can be determined from a curve fitted equations as a function of *S* and length to diameter ratio λ (i.e. $\lambda = L / D$):

$$\varepsilon = \frac{e}{C}. \tag{2.4}$$

The non-dimensional steady state load-carrying components along the line of centers and the perpendicular direction are given by:

$$\bar{w}_r = -0.5 \int_0^{l/2} \int_0^{2\pi} \bar{p}\cos(\theta - \varnothing) d\theta d\bar{z}\,, \tag{2.5}$$

$$\bar{w}_t = 0.5 \int_0^{l/2} \int_0^{2\pi} \bar{p}\sin\left(\theta - \varnothing\right) d\theta d\bar{z}\,. \tag{2.6}$$

The total LCC is calculated as:

$$\overline{w} = \sqrt{\overline{w}_r{}^2 + \overline{w}_t{}^2} \ . \tag{2.7}$$

The non-dimensional LCC and attitude angle are expressed as [16]:

$$\overline{w} = \frac{WC^2}{6\mu UR^2 L} . \tag{2.8}$$

Where W is the applied load, C is the clearance, μ is the lubricant viscosity, U is the surface speed, R is the journal radius and L is the bearing length.
The temperature rise of the lubricant is calculated using:

$$\Delta T = \frac{(2\pi n_s)(fWr)}{\rho Q C_p \left[1 - \frac{1}{2}(Q_s - Q)\right]} \times 10^3 \tag{2.9}$$

where n_s is the rotational speed, f is the friction factor, W is the load, r is the journal radius, ρ is the lubricant density, Q is the flow rate, and C_p is the specific heat of the lubricant.

The average and effective temperatures are determined using the inlet temperature, T_i:

$$T_{av} = T_i + \frac{\Delta T}{2} \quad \text{and} \quad T_e = T_i + 0.8\Delta T \ , \tag{2.10}$$

$$\varnothing = \tan^{-1}\left(\frac{\overline{w}_r}{\overline{w}_t}\right). \tag{2.11}$$

The non-dimensional flow rate is given by:

$$\overline{Q} = \frac{1}{2}\left(\frac{D}{L}\right)^2 \int_0^{2\pi} \overline{h}_0^3 \frac{\partial \overline{P_o}}{\partial \overline{z}} d\theta \ . \tag{2.12}$$

Were $\overline{P_o}$ is the non-dimensional steady-state pressure:

$$\overline{P_o} = \frac{PC^2}{6\mu UR} . \tag{2.13}$$

The friction force is calculated using:

$$\overline{F} = \frac{FC}{\mu URL} = \frac{1}{6}\int_0^{2\pi}\left(\frac{1}{\overline{h}} + 3\overline{h}\frac{\partial \overline{P}}{\partial \theta}\right)\partial\theta . \tag{2.14}$$

The coefficient of friction on the journal surface is represented as:

$$\bar{f} = (R/C)\bar{F} = \frac{\bar{F}}{\bar{w}} = \frac{\int_0^{2\pi}\left(3\bar{h}\frac{\partial \bar{P}_o}{\partial \bar{\theta}} + \frac{1}{h}\right)d\theta}{6\bar{w}}. \tag{2.15}$$

The non-dimensional Sommerfeld number is expressed as:

$$S = \frac{1}{6\pi\bar{w}}. \tag{2.16}$$

The Friction / Power loss in the bearing is given by [19]:

$$F = \frac{2\pi^3 \mu D^3 N^2 L}{C}, \tag{2.17}$$

Dynamic stability,

$$S = \frac{\text{Stiffness} \times \text{Damping}}{\text{Load} - \text{Carrying Capacity}}. \tag{2.18}$$

Where, Stiffness is the bearing's resistance to deformation under load. Damping is the bearing's ability to absorb vibrations and LCC normalizes the stability score for fair comparison across bearings of different capacities [20].

3. Optimization using a MOGA

Optimizing the design of HJBs is a standard multi-objective optimization issue, marked by conflicting objective functions. Multi-objective optimization is a robust approach for pinpointing the optimal set of design variables that achieve the best balance among various performance metrics [21]. Genetic algorithms, a subset of evolutionary algorithms (EAs), are commonly used for solving such problems. Genetic algorithms based on biological evolution and natural selection principles, such as mutation, crossover, and selection, are used to produce optimal solutions [22]. Multi-Objective Genetic Algorithms further build upon this ability by handling multiple objectives concurrently, thereby eliminating the necessity to convert the problem into a series of single-objective optimizations [8]. A Pareto-optimal solution set generated during the bearing design process gives designers the flexibility to choose the most suitable design variables [12].

Real-coded genetic algorithms, which operate with real numbers rather than binary codes, are particularly effective for engineering design problems [8]. The initial step in the GA optimization process involves an initial population of solutions, denoted as chromosomes. A chromosome consists of genes that represent design variables. Within the study's parameters, the population is started with design variables that are feasible within their designated limits, even though some initial solutions may be unachievable according to the set criteria [8, 12]. The steps involved in the Generalised Algorithm process utilised in this study are depicted in Fig.3.

3.1. Formulation of objective functions

The multi-objective optimization function is formulated using a weighted sum approach to combine the stated conflicting objectives which will meet the desired solutions. This is shown in Eq.3.1.

$$F(X) = -w_1(f_1) + w_2(f_2) + w_3(f_3) - w_4(f_4). \tag{3.1}$$

Where f_1, f_2, f_3 and f_4 are represent LCC, temperature rise, friction loss, and stability score respectively. These objective functions are defined in Eqs (2.8), (2.9), (2.17) and (2.18) respectively, Additionally, w_1, w_2, w_3 and w_4 are weights assigned to each objective, reflecting their relative importance. These weights can be adjusted according to specific design requirements and operational goals to tailor the optimization process to desired performance outcomes. The optimisation process takes into account the following constraints based on the given input parameters: a length-to-diameter ratio (*L/D*) of *1*, a clearance (*C*) of *0.05 mm*, an eccentricity ratio (ε) between *0.4* and *0.8*, an applied load (*W*) between *0* and *1500 N*, and a rotational speed (*N*) between *100* and *1500 RPM*. These constraints guarantee that the optimization complies with the practical boundaries of design and operation. Customized changes to HJB designs are made possible through optimization driven by MOGA, thereby meeting performance requirements for enhanced efficiency, stability and dependability [8].

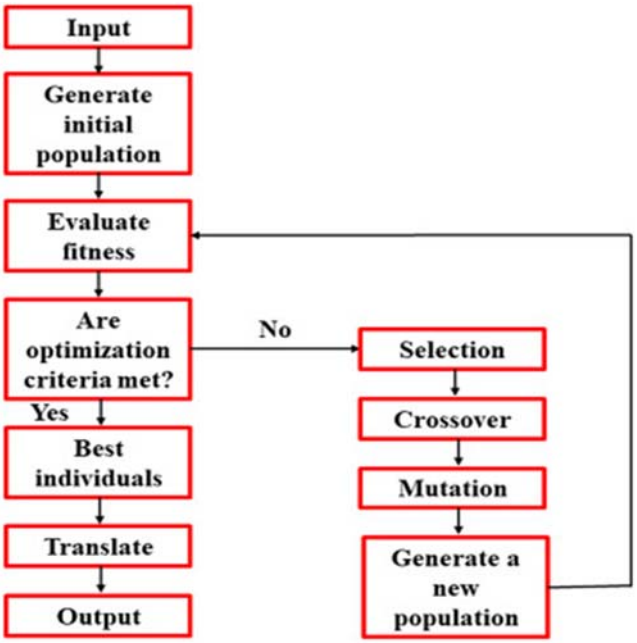

Fig.3. GA process flow chart [23].

3.2. The implementation of a Genetic Algorithm

The optimum design of HJBs represents a typical multi objective optimization problem with conflicting objective functions. The key steps in the genetic algorithm are outlined below and illustrated in the flow chart provided in Fig.3. The various stages of implementation are outlined in the following steps [16].

Step 1: Population of *100* initial solutions is randomly generated, representing combinations of bearing types, eccentricity ratios, clearances and operating speeds. Each solution (chromosome) is encoded as a vector of design variables, including ε , *C*, *N*, *L*, *d* and *D*.

Step 2: The fitness of each chromosome is evaluated using performance metrics such as LCC, Δ*T*, friction loss, and stability. Objectives are normalized using Eq. (3.2).

$$f_{normalized} = \frac{f - f_{min}}{f_{max} - f_{min}}. \tag{3.2}$$

Combine objectives using a weighted sum:

$$F_{total} = -w_1(f_1) + w_2(f_2) + w_3(f_3) - w_4(f_4). \tag{3.3}$$

Step 3: Tournament selection is used to select parent solutions. A random subset of chromosomes is evaluated, and the best-performing solution is chosen as a parent [8].

Step 4: Simulated binary crossover (SBX) is applied with a *90%* probability to generate offspring:

$$O_{offspring\,1} = \alpha X_{parent\,1} + (1-\alpha) X_{parent\,2}, \tag{3.4}$$

$$O_{offspring\,2} = \alpha X_{parent\,2} + (1-\alpha) X_{parent\,1}, \tag{3.5}$$

Step 5: Gaussian mutation is applied with a *10%* probability to introduce random variations:

$$X'_i = X_i + \sigma N(0,1). \tag{3.6}$$

Where σ the mutation step size and N is $(0,1)$ is a Gaussian random variable.

Step 6: Offspring are ranked using Pareto dominance to identify non-dominated solutions [8].

Step 7: Crowding distance is computed to maintain diversity on the Pareto front:

$$D_i = \sum_i \left(\frac{f_j(i+1) - f_j(i-1)}{f_j^{max} - f_j^{min}} \right). \tag{3.7}$$

Step 8: The process terminates after *100* generations or when convergence criteria are met.

Step 9: The MOGA is implemented in Python using libraries such as DEAP for genetic operations, SciPy for numerical computations, NumPy for data handling, and Matplotlib for visualization.

The adopted values for MOGA parameters and HJB design parameters are listed in Tabl.1 and Tab.2, respectively.

Table 1. MOGA process considerations [21, 24].

Parameters	**Values**
Number of generations	*100*
Crossover fraction	*0.8*
Mutation factor	*0.01*
Constraint tolerance	10^{-3}
Function tolerance	10^{-4}

Table 2. HJB design parameters.

Parameter	**Value**
Bearing types	plain, two-lobe, three-lobe, and four-lobe
Bearing diameter *D*	*50 mm*
Journal diameter *d*	*49.89 mm*
L/D ratio	*1*
Clearance c	*0.05 mm*
Bearing material	*C45*, medium carbon steel (*0.42-0.50%*).

Table 2cont. HJB design parameters.

Parameter	**Value**
Journal material (shaft)	*EN8* grade, (*0.36-0.44%*)
Lubricant	MOBIL DTE 24 with *0.5% TiO_2* nanoparticles
Viscosity μ	*0.0292 $Pa \cdot s$* at *40°C*
Density ρ	*0.869 kg/m^3*
Specific heat C_p	*1951 $J / kg \cdot K$*
Inlet oil temperature T_{in}	*40°C*
Initial oil supply pressure P_{si}	*0.4 MPa*
Speed range *N*	*100-1500 RPM*
Eccentricity ratio ε	*0.4-0.8*
Load range *W*	*0-1500 N*

4. MOGA process results

The performance evaluation of HJBs using the MOGA framework revealed significant variations in LCC, temperature rise, friction loss and stability across plain, two-lobe, three-lobe, and four-lobe bearing configurations. The results are presented in Fig.4, which compares the performance parameters across the four bearing types. The Three-Lobe design emerged as the optimal configuration, offering a balanced combination of high LCC, low temperature rise, reduced friction loss, and superior stability. The four-lobe design, while excelling in load capacity, exhibited slightly lower stability due to increased fluid-structure interaction complexity. The two-lobe design provided incremental improvements over plain bearings but fell short of the performance achieved by three-lobe and four-lobe configurations.

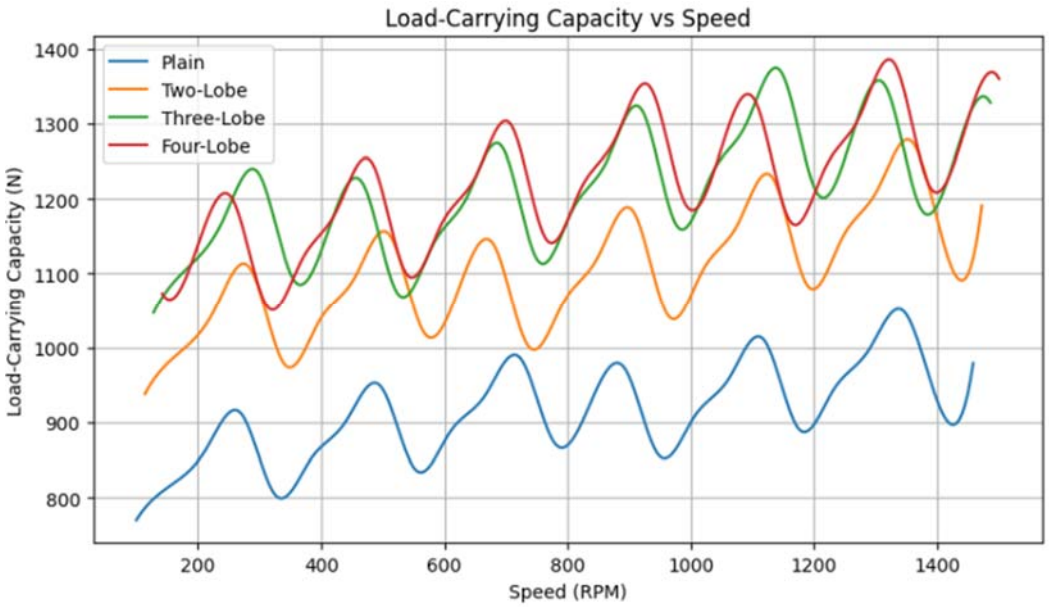

Fig.4(a). Load carrying capacity vs speed.

The Fig.4(a) shows four-lobe bearing exhibited the highest LCC reaching a peak of *1381 N*. This superior performance is attributed to its multiple pressure-building zones, which enhance oil film formation and distribute loads more effectively. The three-lobe bearing followed closely, with a capacity range of *1047-1370 N*, making it the optimal choice for applications requiring a balance between load capacity and stability. In contrast, plain bearings demonstrated the lowest capacity (*770-1050 N*) due to their single pressure-generation zone, which limits hydrodynamic support. The two-lobe design provided intermediate performance (*938-1276 N*), offering improved load distribution compared to plain bearings but falling short of the efficiency achieved by three-lobe and four-lobe designs. The observed increase in load capacity with rotational speed suggests stronger fluid-structure interactions at higher velocities, emphasizing the importance of geometric optimization in high-speed applications.

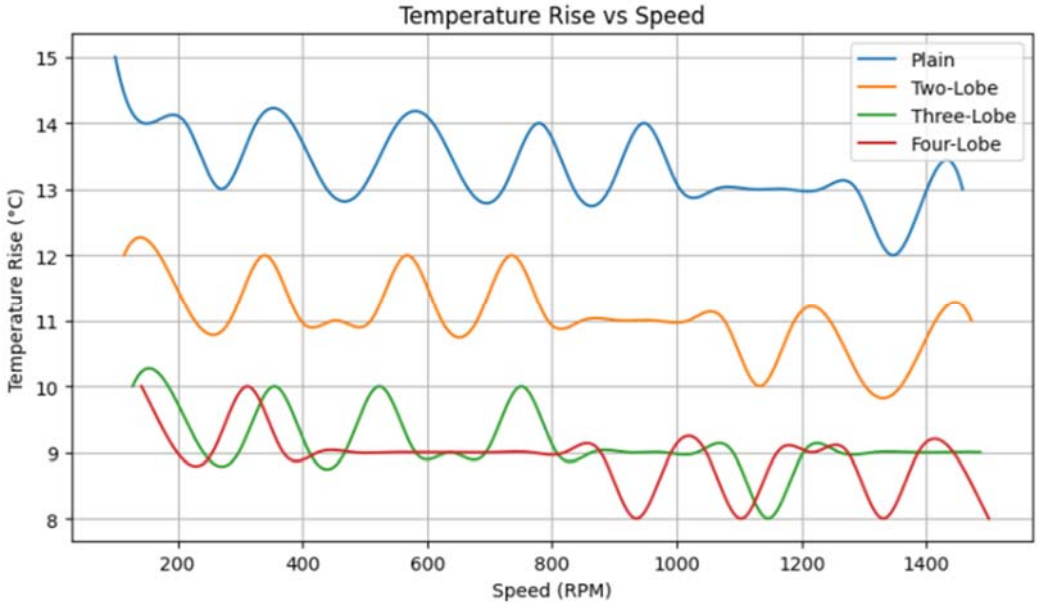

Fig.4(b). Temperature rise vs speed.

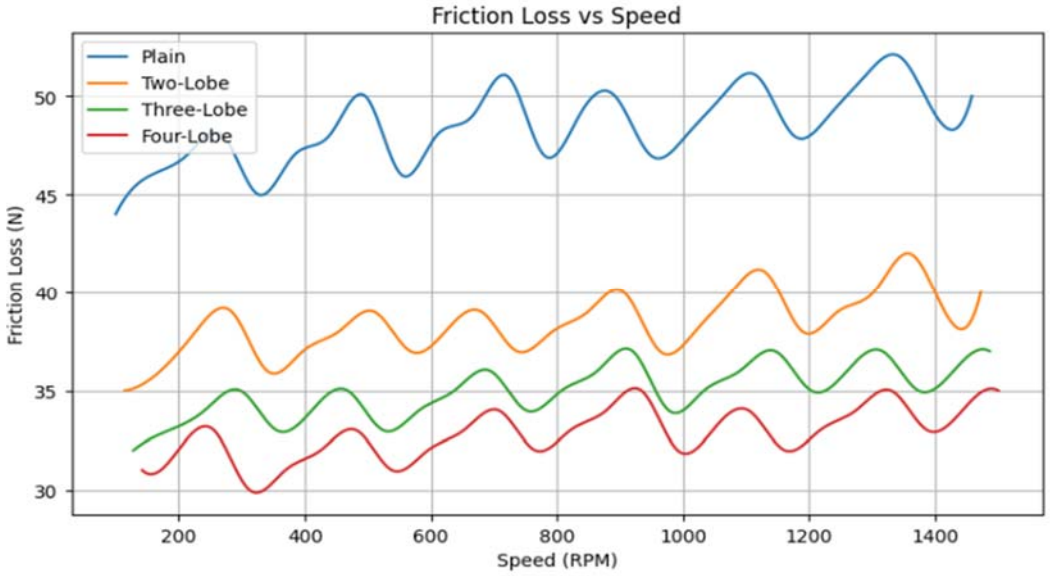

Fig.4(c). Friction loss vs speed.

The Fig.4(b), revealed significant differences in heat dissipation among the bearing configurations. plain bearings experienced the highest temperature rise (*12-15°C*), primarily due to continuous oil film shearing and limited heat dissipation. In contrast, the three-lobe and four-lobe designs maintained significantly lower temperatures (*8-10°C* and *8-12°C*, respectively). Their geometric modifications create multiple oil film breaks, enhancing cooling efficiency and lubricant stability. The two-lobe design exhibited moderate thermal behavior (*10-12°C*), demonstrating incremental improvements in thermal performance as the number of lobes increased. Notably, the three-lobe design achieved a *26.5%* reduction in temperature rise compared to plain bearings, highlighting its superior heat dissipation capabilities.

The Fig.4(c), revealed a direct correlation between bearing geometry and energy dissipation in friction. plain and two-lobe bearings exhibited the highest friction loss (*44-52 N* and *35-42 N*), attributed to continuous oil film shearing and a larger contact area, in contrast, four-lobe bearings minimized friction loss to *30-35 N*, owing to their optimized geometry, which reduces oil film thickness and shear resistance. The three-lobe design reduced friction loss by *29.6%* (*32-37 N*) compared to plain bearings, striking an optimal balance between energy efficiency and load support. The two-lobe bearing showed intermediate friction loss (*35-42 N*), reflecting incremental performance improvements with additional lobes. These findings underscore the importance of geometric design in minimizing energy losses and improving operational efficiency.

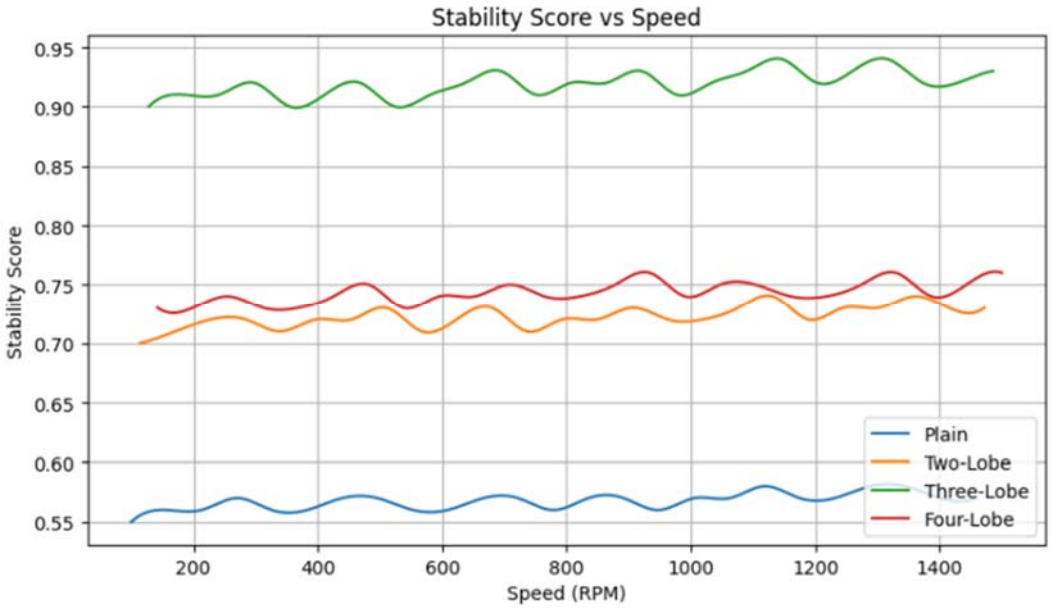

Fig.4(d). Stability score vs speed.

The Fig.4(d), indicated significant variations in dynamic performance across the bearing configurations. The three-lobe design achieved the highest stability score (*0.90-0.94*), improving stability by *46%* over plain bearings (*0.55-0.58*). This enhanced resistance to shaft whirl and dynamic instabilities stems from its three-point pressure support system, which minimizes oil film disruptions and stabilizes rotational motion. The four-lobe design demonstrated good but lower stability (*0.73-0.76*), as its additional lobe increases the complexity of fluid-structure interactions. The two-lobe bearing showed moderate stability (*0.70-0.74*), improving upon the plain bearing but remaining inferior to the three-lobe design. Stability enhancements in multi-lobe configurations suggest better oil film formation and dynamic balance at higher speeds.

The plotted graphs in Figs 4(a) to 4(d) represent interpolated trends derived from discrete simulation data points obtained through the MOGA-based optimization approach. While actual simulations were conducted at specific *RPM* intervals (e.g., *100*, *200*, ..., *1500 RPM*), the continuous nature of the curves has been achieved using interpolation to effectively visualize the overall variation in performance parameters with respect to speed. This graphical representation enhances interpretability and helps identify consistent

behavioral patterns across the full operating range. It is known that experimental investigations generally yield discrete data points. However, the present study focuses on computational optimization and performance prediction, and hence continuous profiles are used to demonstrate the influence of speed on each performance metric. The observed trends are in close agreement with findings reported in the literature and support the superior performance characteristics of multi-lobe bearings particularly the three-lobe configuration as evidenced by studies such as Dhande *et al.* (2018) [6, 7], Biswas *et al.* (2016) [8], and Roy and Kakoty (2014) [22]. These references validate the reliability and practical relevance of the current computational results.

The findings highlight the critical role of geometric design in optimizing the performance of HJBs. Multi-lobe configurations, particularly the three-lobe design, offer significant advantages in terms of load capacity, thermal management, energy efficiency, and stability. These results provide valuable insights for bearing designers and engineers, enabling the selection of optimal configurations based on specific operational requirements. For high-speed and high-load applications, the three-lobe design is recommended for its balanced performance, while the four-lobe design may be preferred for applications prioritizing maximum load capacity.

5. Optimum configuration and operating conditions

The performance evaluation of HJBs across four configurations plain, two-lobe, three-lobe, and four-lobe shown in Tab.3 revealed that the four-lobe design offers the highest LCC (*1218 N*) and the lowest friction loss (*32.5 N*), making it the most effective for maximum load support and energy efficiency. However, the three-lobe bearing demonstrated the best overall performance, with a *9°C* temperature rise (lowest) and the highest stability score (*0.92*), making it the optimal choice for applications requiring a balance of load capacity, thermal efficiency, and dynamic stability. The plain and two-lobe bearings showed inferior performance, with higher temperature rise, friction loss, and lower stability, making them less suitable for demanding industrial applications.

Table 3. Performance metrics values.

Sr. No.	**Performance Parameter**	**Speed (*RPM*)**	**Plain Bearing**	**Two-Lobe**	**Three-Lobe**	**Four-Lobe**	**Optimal Design**	**Key Observations**
1	Load capacity *N*	*100-1500*	*910*	*1107*	*1208*	*1218*	Four-Lobe	Four-Lobe achieves the highest peak capacity, but Three-Lobe has more consistent performance.
2	Temperature rise *°C*		*13.5*	*11*	*9*	*10*	Three-Lobe	Three-Lobe and Four-Lobe offer the best thermal performance. Plain has the highest temperature rise.
3	Friction loss *N*		*48*	*38.5*	*34.5*	*32.5*	Four-Lobe	Friction loss decreases with lobes, with Four-Lobe achieving the lowest.
4	Stability score		*0.56*	*0.72*	*0.92*	*0.74*	Three-Lobe	Three-Lobe offers the best stability, resisting shaft whirl and vibrations.

A speed range of *800-1200 RPM* provides the best compromise between load capacity, stability, and thermal performance, ensuring smooth operation under varying loads. Maintaining the load level at *70-80%* of the maximum capacity ensures a safety margin for dynamic loads, preventing excessive wear and potential failure. Temperature rise should be kept below *10°C* to avoid thermal deformation and ensure consistent

lubricant viscosity, which is critical for maintaining optimal oil film thickness. Additionally, a stability score greater than *0.90* is recommended to minimize vibrations and enhance the bearing's operational lifespan, particularly in high-speed applications.

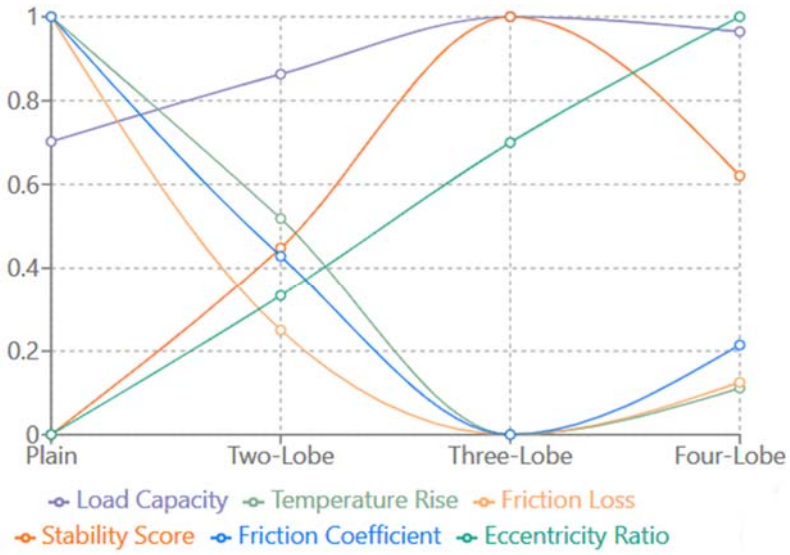

Fig.5. Performance of various parameters with respective types of bearings.

A comparison of the performance metrics for various journal bearings, including plain, two-lobe, three-lobe, and four-lobe types, is presented in Fig.5, with a focus on LCC, temperature rise, friction loss, and stability. The three-lobe bearing leads the way in performance, boasting high load capacity, minimal temperature rise, reduced friction losses, and increased stability. A four-lobe bearing outperforms the other options in terms of load capacity but falls short in terms of thermal and energy efficiency. While plain and two-lobe bearings offer cost advantages, they fall short in terms of their load capacity and stability. A three-lobe configuration was found to be the most suitable option, offering a well-rounded performance in high-joint-balance systems that demand efficiency, reliability, and stability.

The ranking Tab.4 evaluates plain, two-lobe, three-lobe, and four-lobe journal bearings across load capacity, temperature rise, friction loss, and stability. The three-lobe bearing ranks 1^{st} with a total score of *14*, excelling in all metrics, particularly stability and thermal performance, making it the most balanced and reliable choice. The four-lobe bearing also scores *14*, achieving the highest load capacity and lowest friction loss but slightly underperforming in thermal and stability metrics. The two-lobe bearing ranks 3^{rd} with a score of *8*, showing moderate performance but falling short in efficiency and stability. The plain bearing ranks 4^{th} with a score of *4*, performing poorly across all metrics and proving unsuitable for high-performance applications. This ranking underscores the Three-Lobe bearing as the optimal configuration, offering the best balance of performance, efficiency, and reliability for HJBs systems.

The comparative analysis in Fig.6 illustrates the performance trends of plain, two-lobe, three-lobe, and four-lobe bearings across key parameters such as LCC, temperature rise, friction loss, and stability score. The four-lobe bearing demonstrates maximum LCC, making it suitable for heavy-duty applications where high load capacity is the primary requirement. However, its lower thermal efficiency and stability limit its applicability in high-speed or precision systems. The three-lobe bearing shows superior thermal stability and friction management, resulting in more efficient lubrication and reduced wear. Its enhanced stability makes it highly effective in mitigating shaft whirl and dynamic instabilities, ensuring consistent and reliable performance in high-speed operations. Two-lobe bearings offer moderate performance but lack the stability and thermal efficiency needed for demanding applications. Plain bearings, with the lowest stability and highest friction loss, are unsuitable for modern industrial requirements.

Table 4. Performance rankings (Scale: *4* = best, *1* = worst).

Performance Parameter	**Plain Bearing (Rank)**	**Two-Lobe (Rank)**	**Three-Lobe (Rank)**	**Four-Lobe (Rank)**
Load capacity *N*	*1*	*2*	*3*	*4*
Temperature rise *°C*	*1*	*2*	*4*	*3*
Friction loss *N*	*1*	*2*	*3*	*4*
Stability	*1*	*2*	*4*	*3*
Total score	*4*	*8*	*14*	*14*
Rating	***4***	***3***	***1***	***1***

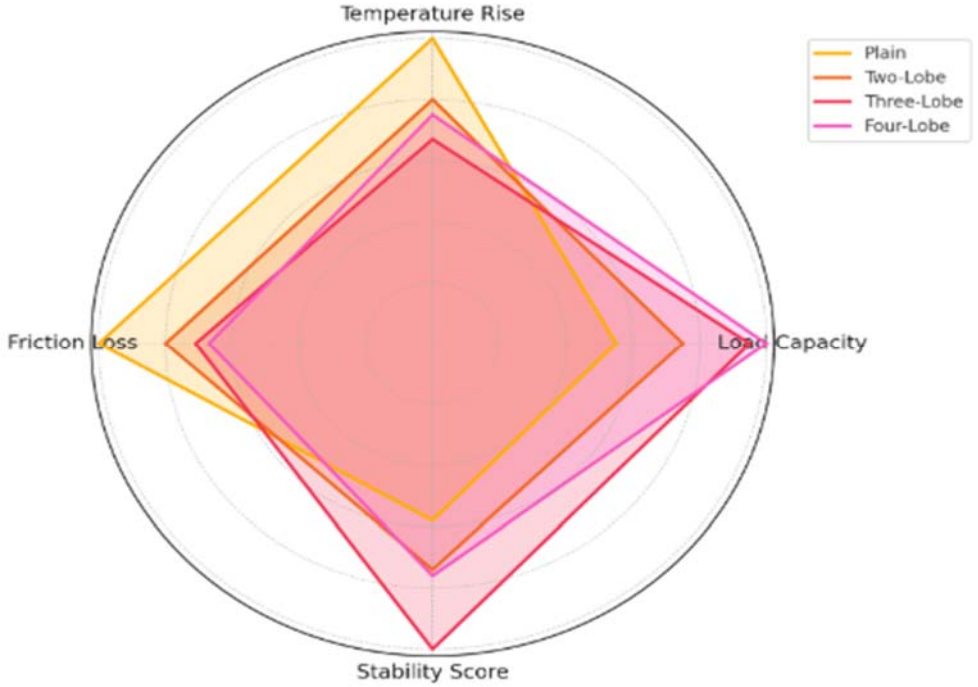

Fig.6. Multi parameter comparisons of considered bearings types.

6. Conclusions

1. The three-lobe bearing configuration proves to be the most advantageous design, striking the perfect balance between load capacity, thermal performance, friction loss, and stability.
2. Its consistent and superior performance makes it the go-to option for high-efficiency applications. A four-lobe bearing offers the highest load capacity and lowest friction loss, though it is narrowly surpassed by a three-lobe design in terms of thermal management and stability, making it best suited for applications prioritizing load handling and energy efficiency.
3. A two-lobe bearing exhibits average performance, surpassing the plain bearing but failing to surpass the three-lobe and four-lobe configurations in terms of efficiency, stability, and thermal performance, thus constraining its suitability for high-performance applications.
4. The plain bearing, although simple and inexpensive, has poor performance in load capacity, heat management, friction, and stability, making it unsuitable for high-performance applications.

This study emphasizes the significance of choosing the right bearing design and operating parameters to strike a balance between performance, efficiency, and longevity in hybrid journal bearing systems.

Future scope

Future studies should focus on advanced lubrication techniques, including the use of lubricants enriched with nanoparticles, self-adjusting lubrication systems, and viscosity formulations that have been optimised, in order to continue improving hydrodynamic performance. Surface engineering techniques, such as Diamond-Like Carbon (DLC) coatings, could enhance wear resistance and reduce energy losses. Additionally, AI-driven multi-objective optimization and real-time condition monitoring should be explored to improve performance under dynamic operating conditions. Large-scale experimental validation will be essential to bridge the gap between theoretical findings and industrial implementation, ensuring that next-generation journal bearings meet the evolving demands of modern engineering applications.

Acknowledgements

We would like to express our sincere gratitude to all those who contributed to the successful completion of this research work. We are also thankful to the faculty members of MET's Institute of Engineering, Nashik, for their constructive feedback and academic sup-port. Lastly, we would like to acknowledge the contributions of various researchers and authors whose published works provided a strong foundation for our study.

Nomenclature

Variables

A – area

C – radial clearance *m*

D – bearing diameter *m*

e – eccentricity *m*

F – friction force *N*

h – oil film thickness *m*

L – bearing length *m*

N – rotational speed *RPM*

F – pressure *Pa*

Q – flow rate m^3/s

R – journal radius *m*

S – Sommerfeld number (dimensionless)

T – temperature °*C*

U – surface speed *m/s*

W – load *N*

X – design variable in genetic algorithm

Index

i – iteration index

j – objective function index

k – generation index

n – population index

s – speed index

Symbols

α – crossover parameter

β – mutation parameter

γ – stability parameter

ΔT – temperature rise $°C$

ε – eccentricity ratio (dimensionless)

ξ – crowding distance

η – efficiency (dimensionless)

θ – angular coordinate *rad*

λ – length-to-diameter ratio (dimensionless)

μ – dynamic viscosity $Pa{\cdot}s$

ζ – damping factor

ρ – lubricant density kg/m^3

σ – mutation step size

ϕ – attitude angle *rad*

ω – angular velocity *rad/s*

Sub symbols

w – total load-carrying capacity N

w_r – load-carrying capacity in radial direction N

w_t – load-carrying capacity in tangential direction N

f – friction factor (dimensionless)

f_1 – LCC objective function

f_2 – temperature rise objective function

f_3 – friction loss objective function

f_4 – stability scores objective function

F_{total} – combined multi-objective optimization function

$F_{normalized}$ – normalized fitness value

References

[1] Abass B., Ahmed S.Y. and Kadhim Z.H. (2023): *Analysis and optimization of nanolubricated journal bearing under thermoelasto-hydrodynamic lubrication considering cavitation effect.*– Tribology in Industry, vol.45, No.4, pp.618-633, https://doi.org/10.24874/ti.1441.01.23.04.

[2] Hirani H. (2004): *Multiobjective optimization of a journal bearing using the Pareto optimality concept.*– Proc. Institution of Mechanical Engineers, Part J: Journal of Engineering Tribology, vol.218, No.4, pp.323-336, https://doi.org/10.1243/1350650041762668.

[3] Bouyer J., Fillon M. and Pierre-Danos I. (2006): *Influence of wear on the behavior of a two-lobe HJB subjected to numerous startups and stops.*– Journal of Tribology - Transactions of the ASME, vol.129, No.2, pp.205-208, https://doi.org/10.1115/1.2401210.

[4] Chen Y., Feng J., Sun Y., Peng X., Dai Q. and Yu C. (2019): *Effect of groove shape on the hydrodynamic lubrication of journal bearing considering cavitation.*– Engineering Computations, vol.37, No.5, pp.1557-1576, https://doi.org/10.1108/EC-06-2019-0287.

[5] Pinkus O. (1956): *Analysis of elliptical bearings*.– Transactions of the American Society of Mechanical Engineers, vol.78, No.5, pp.965-972.

[6] Dhande D.Y., Lanjewar G.H. and Pande D.W. (2018): *Implementation of CFD-FSI technique coupled with response surface optimization method for analysis of three-lobe hydrodynamic journal bearing.*– Journal of the Institution of Engineers (India): Series C, vol.100, No.6, pp.955-966, https://doi.org/10.1007/s40032-018-0492-0.

[7] Dhande D.Y., Pande D.W. and Lanjewar G.H. (2018): *Numerical analysis of three-lobe HJB using CFD-GA technique based on response surface evaluation.*– Journal of the Brazilian Society of Mechanical Sciences and Engineering, vol.40, No.8, https://doi.org/10.1007/s40430-018-1311-5.

[8] Biswas N., Chakraborti P. and Dhar P. (2016): *Optimization of pressure and oil film thickness in multilobe bearing using response surface methodology and MOGA*. – International Journal of Engineering Research and Applications, vol.6, No.3, pp.56-62.

[9] Vinh D.P. (2022): *Effect of loaded-pad thickness on the static behaviors of five-pad hydrodynamic journal bearings*. – Journal of Science and Technology Issue on Information and Communications Technology, pp.15-19, DOI:10.31130/ud-jst.2022.503E.

[10] Shinde A.B. and Pawar P.M. (2017): *Multi-objective optimization of surface textured journal bearing by Taguchi-based Grey relational analysis*. – Tribology International, vol.114, pp.349-357. https://doi.org/10.1016/j.triboint.2017.04.041.

[11] Dang R.K., Goyal D., Chauhan A. and Dhami S.S. (2021): *Numerical and experimental studies on performance enhancement of journal bearings using nanoparticles-based lubricants*.– Archives of Computational Methods in Engineering, pp.1-29, https://doi.org/10.1007/s11831-021-09538-1.

[12] Yang J. and Palazzolo A. (2022): *Deep convolutional autoencoder augmented CFD thermal analysis of bearings with inter pad groove mixing*.– International Journal of Heat and Mass Transfer, vol.188, 122639, https://doi.org/10.1016/j.ijheatmasstransfer.2022.122639.

[13] Yadav S.K., Khatri C.B., Kumar A. and Chaturvedi S. (2024): *Optimization of twin grooved two-lobe textured hydrodynamic journal bearing design by using genetic algorithm.*– Proceedings of the Institution of Mechanical Engineers, Part C: Journal of Mechanical Engineering Science, vol.238, No.20, pp.10205-10221, https://doi.org/10.1177/09544062241256504.

[14] de Castro H.F., de Paula E.H. and Visnadi L.B. (2024): *Reliability-based design optimization applied to a rotor supported by hydrodynamic bearings.*– Machines, vol.12, No.4, p.233, https://doi.org/10.3390/machines12040233.

[15] Zhao J., Li Y., Li Y. and Liu J. (2025): *Multi-objective optimization of tribological properties of diesel engine camshaft bearings.* – Structural and Multidisciplinary Optimization, vol.68, No.1, pp.1-17, DOI:10.1007/s00158-024-03959-9.

[16] Joy N.M. and Roy L. (2016): *Determination of optimum configuration among different configurations of two-axial groove hydrodynamic bearings.*– Proc. Institution of Mechanical Engineers, Part J: Journal of Engineering Tribology, vol.230, No.9, pp.1071-1091, https://doi.org/10.1177/1350650115625604.

[17] Bhagat C. and Roy L. (2014): *Steady state thermo-hydrodynamic analysis of two-axial groove and multilobe hydrodynamic bearings.* – Tribology in Industry, vol.36, No.4.

[18] Das B.J. and Roy L. (2018): *Analysis and comparison of steady-state performance characteristics of two-axial groove and multilobe hydrodynamic bearings lubricated with non-Newtonian fluids.* – Proc. Institution of Mechanical Engineers, Part J: Journal of Engineering Tribology, vol.232, No.12, pp.1581-1596.

[19] Dewangan A., Bhagat S. and Jha V. (2016): *Minimization of power loss in plain journal bearings using genetic algorithms*. – International Journal of Applied Engineering Research, vol.11, No.3, pp.2093-2099.

[20] Zhang Y., He L., Yang J., Zhu G., Jia X. and Yan W. (2021): *Multi-objective optimization design of a novel integral squeeze film bearing damper.*– Machines, vol.9, No.10, p.206, https://doi.org/10.3390/machines9100206.

[21] Shaltout M.L. and Hegazi H.A. (2021): *Multi-objective design optimization of hydrodynamic journal bearings using a hybrid approach*.– Industrial Lubrication and Tribology, vol.73, No.7, pp.1052-1060, https://doi.org/10.1108/ILT-05-2021-0194.

[22] Roy L. and Kakoty S.K. (2014): *Application of genetic algorithm in optimization of hydrodynamic bearings*.– Advances in Intelligent Systems and Computing, pp.207-217, https://doi.org/10.1007/978-81-322-2217-0_18.

[23] Banerjee P., Karri R.R., Mukhopadhyay A. and Das P. (2021): *Review of soft computing techniques for modeling, design, and prediction of wastewater removal performance*. – Soft Computing Techniques in Solid Waste and Wastewater Management, pp.55-73, https://doi.org/10.1016/B978-0-12-824463-0.00005-7.

[24] Deb K., Pratap A., Agarwal S. and Meyarivan T.A.M.T. (2002): *A fast and elitist multiobjective genetic algorithm: NSGA-II*. – IEEE Transactions on Evolutionary Computation, vol.6, No.2, pp.182-197.

Received: March 25, 2025
Revised: September 10, 2025